Microelectronic Engineering 177 (2017) 93–97

Contents lists available at ScienceDirect

Microelectronic Engineering

journal homepage: www.elsevier.com/locate/mee

Focused ion beam implantation for the nucleation of self-catalyzed III-V nanowires

Suzanne Lancaster[a,*], Martin Kriz[a], Markus Schinnerl[a], Donald MacFarland[a], Tobias Zederbauer[a], Aaron Maxwell Andrews[a], Werner Schrenk[a], Gottfried Strasser[a], Hermann Detz[a,b]

[a] Centre for Micro- and Nanostructures, Institute for Solid State Electronics, TU Wien, Vienna 1040, Austria
[b] Austrian Academy of Sciences, Vienna 1010, Austria

ARTICLE INFO

Article history:
Received 18 October 2016
Received in revised form 18 February 2017
Accepted 10 March 2017
Available online 16 March 2017

Keywords:
Nanowires
FIB lithography
MBE
Nanowire arrays
AFM
Photoluminescence
Confocal microscopy

ABSTRACT

Focused ion beam implantation was used for the formation of Ga droplets which act as nucleation points for self-catalyzed, molecular beam epitaxy-grown nanowires on Si(111). In order to further optimize the growth, the substrate after implantation was analyzed via atomic force microscopy, which indicated that sputtering depth had a strong influence on the subsequent nanowire growth. Lower beam voltage accelerations led to beam defocusing and thereafter better growth, while focused, high-acceleration beams led to a larger sputtering depth, worse growth and more tilted nanowire growth. The optical quality of the nanowires was evaluated using spatially resolved photoluminesence measurements at room temperature.

1. Introduction

The integration of III-V materials on silicon is an important area of research today for many electronic and optoelectronic applications [1]. One straightforward way of achieving this integration is in the bottom-up growth of III-V nanowires (NWs), directly on Si substrates, as their unique strain relaxation mechanism allows for the epitaxial growth of lattice mismatched materials [2]. Since III-V NWs are optoelectronic materials, they can be used in applications requiring light absorption and emission [3], and NWs are an effective medium for embedding quantum emitters [4,5], as well as being strong contenders to silicon in electronics due to their high carrier mobilities [6,7].

The application of NWs in more complex geometries and systems requires arrays of single wires at defined positions. These offer several advantages; optical couplings between neighbouring wires can broaden the absorption and transmission spectra [8], also giving them advantages in, for example, solar cells [9]; the number of wires in an array can be controlled to allow scaling for electronic devices [10]; and processing of single-wire devices can be more readily scaled-up on uniform arrays.

Self-catalyzed, bottom-up nanowires are usually nucleated by Ga droplets which self-assemble in random configurations [11], leading to randomly positioned NWs. Therefore, in order to realise positioned arrays, the droplet nucleation needs to be directed. This has been achieved previously via methods such as nanoimprinting gold particles to act as NW catalysts [12], nanosphere lithography of gold droplets [13], or etching holes in an oxide mask via nanoimprint lithography [14] or e-beam lithography [15]. However, since the NW growth method described here is molecular beam epitaxy (MBE) and therefore requires an ultra-high vacuum (UHV) environment, the organic chemicals required for such methods can introduce contaminants into the system if not fully removed. To that end, the method here described is completely free of organic chemicals, and as such is immediately compatible with UHV technology. Additionally, the method lends itself to patterning nanowires on surfaces not easily processed using traditional lithographic methods, such as on tilted facets.

2. Method

The focused ion beam (FIB) implantation method used to nucleate nanowires is shown schematically in Fig. 1 (a). Array points were

* Corresponding author.
E-mail address: suzanne.lancaster@tuwien.ac.at (S. Lancaster).

http://dx.doi.org/10.1016/j.mee.2017.03.003

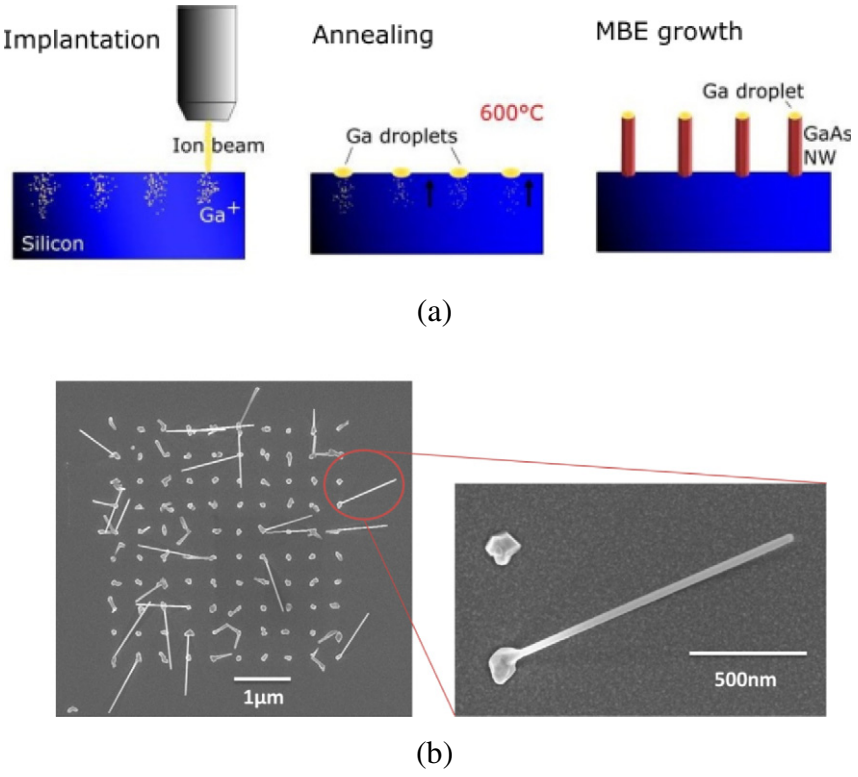

Fig. 1. (a) Schematic of the FIB implantaton array growth method; (b) an early example of an array grown using the method shown in (a), with a close-up of the resulting nanowire growth.

defined via line scans in a Zeiss Neon 40EsB Crossbeam FIB system equipped with a gallium LMIS-FIB (liquid metal ion source), with the beam dwelling at pre-defined points in order to implant Ga^+ ions. In order to characterise the surface damage caused by the implantation step, atomic force microscopy (AFM) images were taken at this point, to measure the topography of the substrate surface. To enhance resolution, AFM measurements were taken in tapping-mode and with a $<$7nm tip radius. During a 600 °C anneal in an UHV environment, Ga^+ ions move to the surface after locally reaching the solubility limit, and form Ga droplets. These droplets can then be used as nucleation points for the growth of nanowires using a self-catalyzed MBE method first described in [16].

Fig. 1 (b) shows an early example of positioned nanowire growth on Si(100) via the method outlined above, thus demonstrating that it is a viable method for the site-controlled growth of NWs. The implantation and subsequent growth can be controlled through tuning of the implantation parameters, ranging from the substrate used, to the acceleration voltage of the FIB, and the dwell time, which affects the number of Ga^+ ions implanted per point. Through parameter optimization, the yield of such arrays has been increased, and to date a vertical NW yield of 82% has been achieved on Si (111) substrates, using a 5 kV focused ion beam. It should be noted that while low acceleration voltages are desirable for nanowire growth, such low voltage beams are more difficult to focus. Further information on the growth method and yield optimization can be found in [17].

In the study described here, we looked at implantation and growth on arrays fabricated on Si(111) substrates. The same wafer was used for arrays implanted at voltages of 5 kV and 30 kV, to reduce discrepancies which could be introduced via slightly differing global conditions during growth. Arrays were implanted at 5 kV or 30 kV and with varying dwell times, leading to varying total ion dose per implantation point. Beam dwell times were varied between 5 and 50 ms, giving a writing speed of 10–100μm/s or 2–20 s per 20×20 array.

After growth, photoluminescence measurements were taken on arrays of nanowires using a Witec confocal microscopy setup. Nanowires were excited by a sapphire laser emitting at 532 nm, and the photoluminescence was collimated with a 100x Nikon objective and analysed using a 600 g /mm spectrometer blazed at 500 nm coupled to an Andor 401 charge coupled device (CCD). The spot size of the setup was nominally 1μm in diameter, a laser output power of 50μW was chosen to minimise damage to the wires via heating [18], and arrays were scanned in 2D by using an automatized xy translation stage.

3. Results

3.1. Growth

The full details of yields achieved for array growth, and the corresponding implantation parameters, are discussed in depth in [17]. We found that the implantation voltage had a large impact on the yield of subsequent nanowire growth, with the maximum yield reaching 82% and 9% for arrays implanted with Ga at 5 kV and 30 kV, respectively, and therefore arrays implanted with these parameters will be analysed in more detail here. Fig. 2 (a) shows a typical GaAs nanowire array, implanted at low (5 kV) beam acceleration voltage. By imaging the arrays along the direction of the beam scan, we can see that the majority of parasitic growth - that is, growth which is off of the array points, as well as multiple nanowires growing on an array point and tilted nanowire growth - is in the direction of the beam scan, with very little parasitic growth in between. This suggests that Ga adatoms which reach the surface during growth are preferentially nucleated at points implanted with Ga, and further that the unwanted growth could be controlled via beam parameters such as dwell times, beam blanking, and beam focusing (as discussed later), while tilted nanowires could be avoided by tweaking the growth parameters [19].

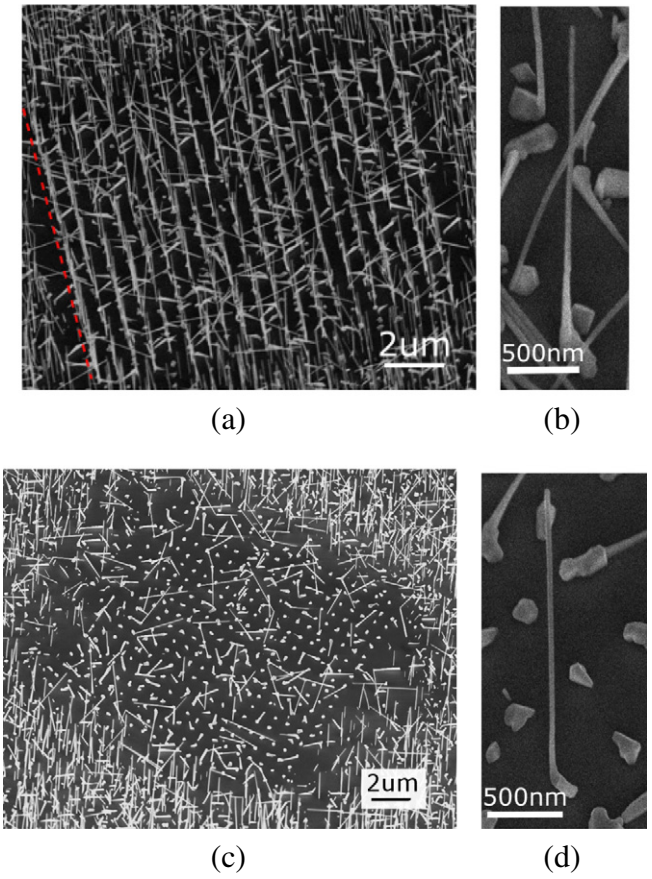

Fig. 2. SEM images of array growth and individual wire growth after FIB implantation at (a), (b) 5kV and (c), (d) 30kV. In (a) the beam scan direction is indicated by a dotted line.

For comparison, we include an image of an array where the Ga^+ was implanted at 30 kV, as well as the surrounding substrate (Fig. 2 (c)). Despite the fact that Ga droplets clearly formed well on the array points, subsequent nanowire growth was poor, as mentioned above. There is also, however, little parasitic growth within the implantation area (i.e. random nanowire growth was suppressed), and many of the wires which did grow are tilted. Notably, when an implantation acceleration voltage of 30 kV is used, nanowire growth is also sparser in the area directly surrounding the array.

3.2. Surface characterization after implantation

To further investigate the effect of the FIB on the growth substrate, and to understand how this influences the growth, AFM images of the implanted Ga^+ arrays were taken in between the patterning and annealing steps. Some representative AFM images taken for 5 kV- and 30 kV-implanted arrays are shown in Fig. 3 (a) & (b). As mentioned earlier, the beam focusing becomes more difficult as we move to lower acceleration voltages; this beam defocusing is clearly visible in Fig. 3 (a) and can help to explain the increased parasitic growth described above and shown in Fig. 2 (a), as there is a broadening of the implantation point in the direction of the beam scan.

By comparing the AFM profiles of individual implantation points (Fig. 3 (c)), we can see that the sputtering depth of impinging ions from the beam is much higher for the 30 kV beam than for the 5 kV beam (1.73 nm and 0.49 nm, respectively). Since the sputtering depth is directly related to the beam current profile [20], this confirms that the 5 kV beam is defocused. The total ion dose per implantation point depended on the beam current, which is fixed for each acceleration voltage, and the beam dwell time. The results discussed here and shown in Figs. 2 & 3 are for doses chosen to give the highest nanowire growth yields. If the beam is defocused, we can assume that the total ion dose (as determined by dwell time) is spread over a larger area and therefore the local dose is lower. This could help to explain the discrepancy between optimal doses for the 5 kV and 30 kV cases, and should be investigated further via intentional defocusing of the 30 kV beam. It is also interesting to note the large proportion of tilted nanowires in Fig. 2 (c). This could suggest that the sputtering visible in the AFM images leaves various crystal planes exposed from which NWs are nucleated.

From SRIM simulations (the Stopping and Range of ions in Matter, [21]), we calculated the mean stopping distance of Ga+ ions in Si, which we found to vary from 8.1 nm for a 5 kV beam to 26.9 nm for a 30 kV beam. Deviations in the incidence angle, which we would assume to occur for the unfocused beam, slightly reduce the maximum stopping distance of the 5 kV beam, to 7 nm for a 30° angle of incidence. The increased implantation depth for 30 kV arrays could be considered as a reason for the lower nucleation rates of nanowires in this case, however, from Fig. 2 (c) we can clearly see that droplets have formed on all array points, suggesting that sufficient Ga+ ions reached the surface upon annealing.

Self-catalyzed nanowire growth is known to be heavily influenced by the III/V ratio during growth [19], the presence of a SiO_2 layer on the substrate [16], and the growth temperature [22], yet the arrays discussed in this paper were grown on the same wafer and therefore under the same global conditions. The absence of good nanowire growth in certain arrays would suggest that local conditions varied across the substrate, further evidence for which is the onset of normal growth off of the array, at the edges of Fig. 2 (c). One explanation could be that Ga enriched areas arising from the higher implantation depth of the 30 kV beam lead to temperature fluctuations in the region, as the growth depends sensitively on temperature [23], and a change of several °C could be critical in determining the growth of nanowires.

3.3. Optical characterization of nanowires

Fig. 4 (a) shows a photoluminescence (PL) map of a typical array at an emission energy of 1.42 eV (the room temperature bandgap of GaAs [24]). The majority of NWs are optically active, even without a shell, which indicates good crystal structure in the wires, and since the emission could be further enhanced by capping with e.g. a conformal AlGaAs shell [25], this is a promising result for the integration of such arrays in optoelectronics.

Individual PL spectra corresponding to the bright spots indicated in 4(a) are shown in Fig. 4 (b). We see a variation in the emission energy, from just above the expected bandgap to 100 meV above bandgap, which is consistent with literature values [25,26]. The broad emission could be attributed to a tapering in the nanowires as visible in 2(b), and could also be indicative of a mix of wurtzite & zinc-blende crystal structure within the NWs [27], as well as thermal broadening due to measuring at room temperature.

The PL map and individual scans shown are from nanowires grown on an array implanted at 5 kV. Nanowires on arrays implanted at 30 kV were also optically active and showed similar PL. This suggests that once nanowires were nucleated, they grew with similar crystal structures and morphologies.

4. Conclusions & outlook

The results presented here demonstrate that FIB-implanted gallium can be viably used for the nucleation of positioned, self-

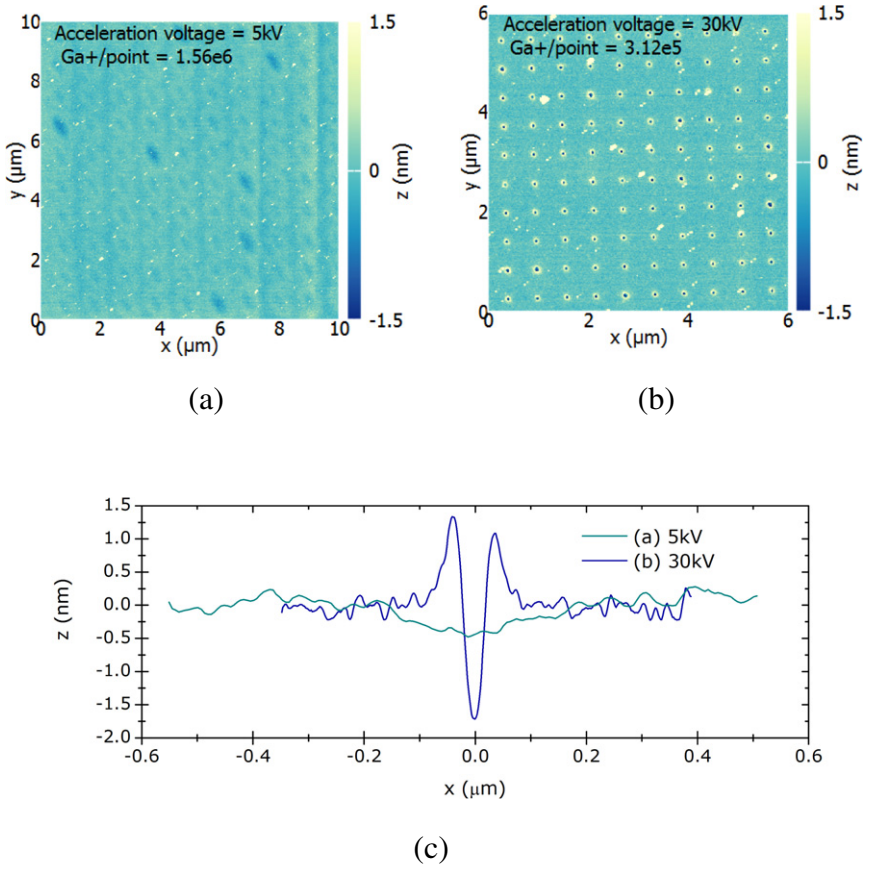

Fig. 3. AFM images of Si(111) surface after Ga^+ implantation at (a) 5 kV and (b) 30 kV. For the 5 kV sample the dose shown was the lowest where features were visible in AFM, and the pitch was increased for clarity. (c) Line scans across implantation points for the arrays shown in (a) and (b).

catalyzed III-V nanowires on silicon. While beam parameters have currently been optimised to produce a high vertical nanowire yield on Si(111) substrates, the problem of unwanted parasitic growth persists.

There are two factors which have a striking influence on the implantation step for the nucleation of good, uniform wires. The first is the focus of the beam, as an unfocused beam leads to implantation over a large area and therefore unwanted growth beyond the defined array points. Secondly, surface analysis after implantation seems to indicate that deep sputtering arising from a high acceleration voltage does not affect the number of droplets nucleated on array sites, and therefore cannot be directly linked to a decrease in nanowire yield, but does lead to the growth of tilted nanowires via exposure of additional crystal planes. Further, we hypothesise that deep implantation of Ga, as with higher acceleration voltages, leads to temperature fluctuations which affect growth on the arrays and the surrounding substrate. This is avoided with lower acceleration voltages as the implantation depth is lower, as is the local dose due to the aforementioned beam defocusing.

The lack of any required pre-patterning or alignment steps makes this method highly versatile, as it could be used to nucleate NWs in any configuration and on different substrates. Nanowires grown via this method were optically active even at room temperature, pointing to their good quality and demonstrating that the arrays could be used in optical and optoelectronic devices such as photovoltaics, lasers and detectors.

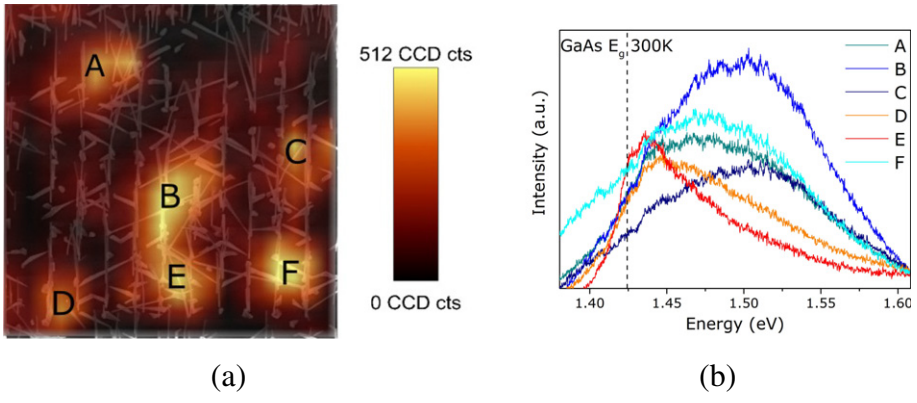

Fig. 4. (a) Room temperature PL map of an array with 76% yield, at an emission energy of 1.42eV; (b) individual PL spectra from the bright spots marked in (a).

Acknowledgments

The authors would like to thank the Austrian Science Fund (FWF): P26100-N27 (H2N) for funding. HD acknowledges financial support through an APART fellowship from the Austrian Academy of Sciences.

References

[1] K. Tanabe, K. Watanabe, Y. Arakawa, III-V/Si hybrid photonic devices by direct fusion bonding, Sci. Rep. 2 (2012) 349.
[2] T. Mårtensson, C.P.T. Svensson, B.A. Wacaser, M.W. Larsson, W. Seifert, K. Deppert, A. Gustafsson, L.R. Wallenberg, L. Samuelson, Epitaxial III-V nanowires on silicon, Nano Lett. 4 (10) (2004) 1987–1990.
[3] T. Stettner, P. Zimmermann, B. Loitsch, M. Döblinger, A. Regler, B. Mayer, J. Winnerl, S. Matich, H. Riedl, M. Kaniber, et al. Coaxial GaAs-AlGaAs core-multishell nanowire lasers with epitaxial gain control, Appl. Phys. Lett. 108 (1) (2016) 011108.
[4] M.T. Borgström, V. Zwiller, E. Müller, A. Imamoglu, Optically bright quantum dots in single nanowires, Nano Lett. 5 (7) (2005) 1439–1443.
[5] M. Makhonin, A. Foster, A. Krysa, P. Fry, D. Davies, T. Grange, T. Walther, M. Skolnick, L. Wilson, Homogeneous array of nanowire-embedded quantum light emitters, Nano Lett. 13 (3) (2013) 861–865.
[6] T. Bryllert, L.-E. Wernersson, L. Froberg, L. Samuelson, Vertical high-mobility wrap-gated InAs nanowire transistor, IEEE Electron Device Lett. 27 (5) (2006) 323–325.
[7] J.B. Kinzel, F.J.R. Schülein, M. Weiß, L. Janker, D.D. Bühler, M. Heigl, D. Rudolph, S. Morkötter, M. Döblinger, M. Bichler, G. Abstreiter, J.J. Finley, A. Wixforth, G. Koblmüller, H.J. Krenner, The native material limit of electron and hole mobilities in semiconductor nanowires, ACS Nano 10 (5) (2016) 4942–4953.
[8] L. Cao, P. Fan, M.L. Brongersma, Optical coupling of deep-subwavelength semiconductor nanowires, Nano lett. 11 (4) (2011) 1463–1468.
[9] L. Wen, Z. Zhao, X. Li, Y. Shen, H. Guo, Y. Wang, Theoretical analysis and modeling of light trapping in high efficiency GaAs nanowire array solar cells, Appl. Phys. Lett. 99 (14) (2011) 143116.
[10] C. Black, Self-aligned self assembly of multi-nanowire silicon field effect transistors, Appl. Phys. Lett. 87 (16) (2005) 163116.
[11] H. Detz, M. Kriz, D. MacFarland, S. Lancaster, T. Zederbauer, M. Capriotti, A. Andrews, W. Schrenk, G. Strasser, Nucleation of Ga droplets on Si and SiOx surfaces, Nanotechnology 26 (31) (2015) 315601.
[12] T. Mårtensson, P. Carlberg, M. Borgström, L. Montelius, W. Seifert, L. Samuelson, Nanowire arrays defined by nanoimprint lithography, Nano Lett. 4 (4) (2004) 699–702.
[13] B. Fuhrmann, H.S. Leipner, H.-R. Höche, L. Schubert, P. Werner, U. Gösele, Ordered arrays of silicon nanowires produced by nanosphere lithography and molecular beam epitaxy, Nano Lett. 5 (12) (2005) 2524–2527.
[14] A.M. Munshi, D.L. Dheeraj, V.T. Fauske, D.-C. Kim, J. Huh, J.F. Reinertsen, L. Ahtapodov, K. Lee, B. Heidari, A. Van Helvoort, et al. Position-controlled uniform GaAs nanowires on silicon using nanoimprint lithography, Nano lett. 14 (2) (2014) 960–966.
[15] B. Bauer, A. Rudolph, M. Soda, A.F. i Morral, J. Zweck, D. Schuh, E. Reiger, Position controlled self-catalyzed growth of GaAs nanowires by molecular beam epitaxy, Nanotechnology 21 (43) (2010) 435601.
[16] A. Fontcuberta i Morral, C. Colombo, G. Abstreiter, J. Arbiol, J. Morante, Nucleation mechanism of gallium-assisted molecular beam epitaxy growth of gallium arsenide nanowires, Appl. Phys. Lett. 92 (6) (2008) 063112.
[17] H. Detz, M. Kriz, S. Lancaster, D. MacFarland, M. Schinnerl, T. Zederbauer, A. Andrews, W. Schrenk, G. Strasser, Lithography-free positioned GaAs nanowire growth with focused ion beam implantation of Ga, J. Vac. Sci. Technol. B 35 (1) (2017) 011803.
[18] M. Heiss, S. Conesa-Boj, J. Ren, H.-H. Tseng, A. Gali, A. Rudolph, E. Uccelli, F. Peiró, J.R. Morante, D. Schuh, Direct correlation of crystal structure and optical properties in wurtzite/zinc-blende GaAs nanowire heterostructures, Phys. Rev. B 83 (4) (2011) 045303.
[19] F. Bastiman, H. Küpers, C. Somaschini, L. Geelhaar, Growth map for Ga-assisted growth of GaAs nanowires on Si (111) substrates by molecular beam epitaxy, Nanotechnology 27 (9) (2016) 095601.
[20] A. Lugstein, B. Basnar, G. Hobler, E. Bertagnolli, Current density profile extraction of focused ion beams based on atomic force microscopy contour profiling of nanodots, J. Appl. Phys. 92 (7) (2002) 4037–4042.
[21] J.F. Ziegler, M.D. Ziegler, J.P. Biersack, SRIM-The stopping and range of ions in matter (2010), Nucl. Instrum. Methods Phys. Res. Sec. B: Beam Interact. Mater. Atoms 268 (11) (2010) 1818–1823.
[22] P. Krogstrup, R. Popovitz-Biro, E. Johnson, M.H. Madsen, J. Nygård, H. Shtrikman, Structural phase control in self-catalyzed growth of GaAs nanowires on silicon (111), Nano lett. 10 (11) (2010) 4475–4482.
[23] G. Cirlin, V. Dubrovskii, I. Soshnikov, N. Sibirev, Y.B. Samsonenko, A. Bouravleuv, J. Harmand, F. Glas, Critical diameters and temperature domains for MBE growth of III-V nanowires on lattice mismatched substrates, Phys. Status Solidi RRL 3 (4) (2009) 112–114.
[24] Y. Lee, A. Chavez-Pirson, S.W. Koch, H. Gibbs, S. Park, J. Morhange, A. Jeffery, N. Peyghambarian, L. Banyai, A. Gossard, et al. Room-temperature optical nonlinearities in GaAs, Phys. Rev. Lett. 57 (19) (1986) 2446.
[25] L. Titova, T.B. Hoang, H. Jackson, L. Smith, J. Yarrison-Rice, Y. Kim, H. Joyce, H. Tan, C. Jagadish, et al. Temperature Dependence of Photoluminescence from Single Core-shell GaAs-AlGaAs Nanowires, 2006.
[26] J. Motohisa, J. Noborisaka, J. Takeda, M. Inari, T. Fukui, Catalyst-free selective-area {MOVPE} of semiconductor nanowires on (111)B oriented substrates, J. Cryst. Growth 272 (1–4) (2004) 180–185. the Twelfth International Conference on Metalorganic Vapor Phase Epitaxy.
[27] D. Spirkoska, J. Arbiol, A. Gustafsson, S. Conesa-Boj, F. Glas, I. Zardo, M. Heigoldt, M. Gass, A.L. Bleloch, S. Estrade, et al. Structural and optical properties of high quality zinc-blende/wurtzite GaAs nanowire heterostructures, Phys. Rev. B 80 (24) (2009) 245325.